Biophysical *Journal*
Article

Biophysical Society

# Membrane Solubilization by Styrene-Maleic Acid Copolymers: Delineating the Role of Polymer Length

Juan J. Domínguez Pardo,[1,*] Martijn C. Koorengevel,[1] Naomi Uwugiaren,[1] Jeroen Weijers,[1] Adrian H. Kopf,[1] Helene Jahn,[1] Cornelis A. van Walree,[1] Mies J. van Steenbergen,[2] and J. Antoinette Killian[1,*]
[1]Membrane Biochemistry & Biophysics, Bijvoet Center for Biomolecular Research, Department of Chemistry, and [2]Department of Pharmaceutics, Utrecht Institute for Pharmaceutical Sciences, Faculty of Science, Utrecht University, Utrecht, the Netherlands

ABSTRACT Styrene-maleic acid (SMA) copolymers have attracted interest in membrane research because they allow the solubilization and purification of membrane-spanning proteins from biological membranes in the form of native-like nanodisks. However, our understanding of the underlying SMA-lipid interactions is hampered by the fact that SMA preparations are very polydisperse. Here, we obtained fractions of the two most commonly used SMA preparations: SMA 2:1 and SMA 3:1 (both with specified $M_w$ ~10 kD), with different number-average molecular weight ($M_n$) and styrene content. The fractionation is based on the differential solubility of styrene-maleic anhydride (SMAnh) in hexane and acetone mixtures. SMAnh fractions were hydrolyzed to SMA and added to lipid self-assemblies. It was found that SMA fractions inserted in monolayers and solubilized vesicles to a different extent, with the highest efficiency being observed for low-$M_n$ SMA polymers. Electron microscopy and dynamic light scattering size analyses confirmed the presence of nanodisks independent of the $M_n$ of the SMA polymers forming the belt, and it was shown that the nanodisks all have approximately the same size. However, nanodisks bounded by high-$M_n$ SMA polymers were more stable than those bounded by low-$M_n$ polymers, as indicated by a better retention of the native lipid thermotropic properties and by slower exchange rates of lipids between nanodisks. In conclusion, we here present a simple method to separate SMAnh molecules based on their $M_n$ from commercial SMAnh blends, which allowed us to obtain insights into the importance of SMA length for polymer-lipid interactions.

## INTRODUCTION

Styrene-maleic acid (SMA) copolymers are in the spotlight of membrane protein research because of their ability to solubilize lipid membranes into nanodisks (for reviews, see (1,2)). SMA-mediated solubilization offers many advantages over conventional solubilization methods based on the use of detergents, including retention of the membrane architecture (i.e., lipid bilayer conformation) in nanodisks (3,4) and the suitability of nanodisk particles for analysis by biophysical techniques such as NMR (5,6), turbidimetry (7,8), and calorimetry (3,9,10).

A broad range of SMA polymers differing in composition and in length are commercially available. It has been shown that the composition of the SMA polymers strongly affects the membrane solubilization properties in model membranes (11) as well as in biological membranes (12,13) and that it also affects the properties of the resulting nanodisks (9). Recently, also the effect of polymer length in membrane solubilization has been investigated. It was found that the solubilization of a broad range of membrane-spanning proteins (i.e., BmrA, LeuT, ZipA) from *Escherichia coli* membranes was most efficiently conducted by low-molecular-weight (~6–10 kDa) SMA polymers (13). Similarly, it was found that low-molecular-weight SMA polymers were able to solubilize *Rhodobacter sphaeroides* monomeric reaction centers ~3× more efficiently than their high-molecular-weight SMA counterparts (12). However, our understanding of the underlying SMA-lipid interactions is hampered by the fact that SMA preparations are very polydisperse and consist of a broad variety of SMA polymers with different lengths and compositions (11). This also holds for the lowest-molecular-weight polymers, and thus it is possible that a subset of even smaller polymers is most effective in solubilization.

To gain further insight into how length and composition of the SMA polymers affect membrane solubilization and

*Submitted February 27, 2018, and accepted for publication May 21, 2018.*
*Correspondence: j.j.dominguezpardo@gmail.com or j.a.killian@uu.nl
Editor: Tommy Nylander.
https://doi.org/10.1016/j.bpj.2018.05.032

the properties of the resulting nanodisks, we here prepared subfractions of the two most commonly used blends of SMA. These are preparations with styrene/maleic acid ratios of 2:1 and 3:1, denoted as SMA 2:1 and SMA 3:1, respectively, with a relatively low average molecular weight. The fractionation was based on differential solubility of the non-hydrolyzed polymer forms (i.e., styrene-maleic anhydride, SMAnh) in hexane and acetone mixtures. For each SMAnh preparation, we obtained four pools of polymers with different number-average molecular weight ($M_n$) values in the range of 1.1–6.5 kDa, and each was hydrolyzed to SMA. It was found that low-$M_n$ SMA polymers insert to the highest extent into phosphatidylcholine monolayers. Similarly, the solubilization of phosphatidylcholine vesicles was found to be most efficiently conducted by low-$M_n$ SMA. All SMA polymer fractions were found to yield nanodisks with no apparent size correlation with the length or with the composition of the polymer belt. However, the length of the polymer belt does seem to affect the stability of the enclosed lipids. The highest perturbation of the thermotropic properties of the lipids and the fastest lipid exchange rates between nanodisks were found when these are bounded by low-$M_n$ SMA polymers. Overall, the fragments derived from SMA 2:1 polymers yielded a better stability than the fragments derived from SMA 3:1 polymers. In conclusion, we here present a simple method to separate high-$M_n$ and low-$M_n$ SMAnh polymers from commercial SMAnh mixtures, providing more insights into the effects of polymer length on membrane solubilization.

## MATERIALS AND METHODS

### Materials

1,2-dimyristoyl-*sn*-glycero-3-phosphocholine (di-14:0 PC), 1,2-dipalmitoyl-*sn*-glycero-3-phosphocholine (di-16:0 PC), 1,2-distearoyl-*sn*-glycero-3-phosphocholine (di-18:0 PC), and 1,2-dimyristoyl-*sn*-glycero-3-phosphoethanolamine-N-(lissamine rhodamine B sulfonyl) were purchased from Avanti Polar Lipids (Alabaster, AL). SMAnh copolymers Xiran 30010 (molar ratio of styrene/maleic anhydride of 2:1) and Xiran 25010 (molar ratio of styrene/maleic anhydride of 3:1), both with a weight-average molecular weight of ~10 kDa, were a kind gift from Polyscope Polymers (Geleen, The Netherlands). All other chemicals were purchased from Sigma-Aldrich (St. Louis, MO).

### Fragmentation of SMAnh copolymers

SMAnh copolymers were fragmented by differential solubilization as follows. A 10% (w/w) solution of SMAnh 2:1 (i.e., X30010) or SMAnh 3:1 (i.e., X25010) in acetone was mixed with an equal volume of hexane to a final 50% (v/v) concentration and centrifuged for 10 min at 10,000 × *g* at 4°C, leading to the formation of a two-layer system. The bottom layer, denoted the SMAnh P50 fraction, and the upper layer were separated by pipette aspiration and dried by rotary evaporation of the solvents. The residue of the upper layer was dissolved in 10% (w/w) acetone, and hexane was added to a final concentration of 80% (v/v). The resulting mixture was centrifuged for 10 min at 10,000 × *g* at 4°C, leading to the separation of the pellet (denoted the SMAnh P80 fraction) from the supernatant. This procedure was repeated for a final concentration of 90% (v/v) hexane, yielding the SMAnh P90 fraction, and then for a final concentration of 96.5% (v/v) hexane, yielding the SMAnh P96 fraction (denoted SMAnh P96 instead of SMAnh P96.5 for legibility). To remove any trapped soluble material in the pellet fractions, an additional washing step was done as follows: 10% (w/w) SMAnh solutions consisting of P50, P80, P90, and P96 in acetone were mixed with hexane to a final 51, 81, 91, and 97% (v/v) hexane concentration, respectively. The mixtures were centrifuged for 20 min at 10,000 × *g* at 4°C. The supernatants were discarded, and the pellets were dried by rotary evaporation and used for further analysis. The supernatant fraction obtained upon 96% hexane addition was also discarded because it did not yield a soluble fraction upon hydrolysis and was found to be completely inactive in solubilization experiments. Most likely this fraction mainly contained styrene-rich byproducts from the polymerization reaction.

### Ultraviolet-visible spectroscopy

Ultraviolet-visible spectra were obtained for 1 mL aliquots of 0.0125% (w/v) SMAnh solutions in tetrahydrofuran (THF). SMAnh solutions were transferred to a quartz cuvette and equilibrated at 25°C for 1 min. Scans were recorded in the range of 240–290 nm at a speed of 120 nm/min using a Lambda 18 spectrophotometer (PerkinElmer, Waltham, MA). Data points were obtained every 0.25 nm.

### Gel permeation chromatography

50 μL aliquots of 0.2% (w/v) SMAnh solutions in THF were analyzed with a Waters Alliance 2695 system (Milford, MA) and a Waters 2410 RI detector. An Agilent PL gel Mesopore column 8 × 300 mm (Santa Clara, CA) at a temperature of 30°C was used with THF at a constant flow rate of 1 mL/min as eluent. Data collection and analysis were done with Empower 3 software (Waters). $M_n$ values of the different SMAnh fractions were obtained by relative calibration using polystyrene standards (14).

### Preparation of SMA fragments

SMAnh fragments were converted to the acid form by alkaline hydrolysis as follows: 10% (w/v) SMAnh suspensions in water containing 0.6 equivalents of NaOH (NaOH-to-carboxylic acid groups, mol) were introduced in a Certoclav pressure cooker (Traun, Austria) and were subjected to at least 3 × 15 min autoclave cycles at 125°C. Additional aliquots of NaOH 1 M solution were further added if necessary until the desired pH (7.8–8) was reached.

### Size-exclusion chromatography

100 μL of 0.5% (w/v) SMA solutions in 2 mM Britton-Robinson buffer (pH 8.0) were injected into a manually prepared Sephadex G-75 column (32 × 2 cm) equipped with an Akta purification system (Chicago, IL). Size-exclusion chromatography (SEC) chromatograms were obtained at a flow rate of 0.2–1 mL/min.

### Fourier-transform infrared spectroscopy

Fourier-transform infrared spectroscopy (FTIR) spectra were recorded for the different SMAnh fractions using a Perkin-Elmer Spectrum 100 FT-IR spectrometer operated by Perkin-Elmer Spectrum software version 10.4.449. Spectra were collected in the ATR mode. Relative styrene/maleic acid ratios were obtained from the ratio $A_{680\ cm-1}/A_{1780\ cm-1}$, corresponding to the vibration modes of CH-$sp^2$ bending of monosubstituted benzene at 680 $cm^{-1}$ and to the vibration mode of C=O anhydride stretching at 1780 $cm^{-1}$.

## Lipid monolayer experiments

Surface-pressure isotherms versus time were recorded for lipid monolayers formed of either di-14:0 PC or di-18:0 PC upon addition of 20 $\mu$L SMA 10% w/v (yielding a final concentration of 0.01% w/v). Phospholipid monolayers were assembled on a 6.0 $\times$ 5.5 cm compartment of a homemade Teflon trough filled with 20 mL buffer (Tris HCl 50 mM, NaCl 150 mM (pH 8.0)). Aliquots from 2.5 mM phospholipid stock solutions in chloroform/methanol (9:1 v/v) were carefully added dropwise to the surface of the buffer solution until an initial surface pressure of 25 mN/m was reached. SMA was added after 2 min of stabilization, and the increase in surface pressure was recorded for at least 30 min using a MicroTrough XS monolayer system (Kibron, Helsinki, Finland). Surface-pressure isotherms presented in this study are a result of the average of two independent experiments. All experiments were conducted at room temperature.

## Preparation of multilamellar vesicles

Phospholipid stock solutions were prepared in chloroform/methanol (9:1 v/v) in concentrations of 10 mM based on phosphate analysis (15). Aliquots from the phospholipid stock solutions were taken, and the solvent was removed under a stream of $N_2$. The resulting lipid film was dried in a desiccator under vacuum for at least 1 hr. Next, the lipid films were hydrated with buffer (Tris-HCl 50 mM, NaCl 150 mM (pH 8.0)) to the desired final concentration and stabilized for at least 5 min at T > melting temperature ($T_m$). The samples were then subjected to 10 freeze-thaw cycles, each consisting of 3 min freezing in liquid $N_2$ (−196°C) and 3 min thawing in a water bath at 60°C, well above the $T_m$ of the lipids (16).

## Kinetics of solubilization of phosphatidylcholine vesicles

700 $\mu$L aliquots of 0.5 mM dispersions of di-14:0 PC multilamellar vesicles (MLVs) in solubilization buffer (Tris-HCl 50 mM, NaCl 150 mM (pH 8.0)) were mixed with SMA 5% (w/v) to a final SMA/lipid mass ratio ~3.0. Solubilization kinetics were followed at a fixed wavelength of 350 nm by monitoring the decrease of the apparent absorbance. The solubilization process was recorded for 15 min at 15°C, which is below the $T_m$ of di-14:0 PC ($T_m \sim 23$°C) (16). The temperature was controlled with a Peltier cuvette holder (Santa Clara, CA). Absorbance values were recorded every 0.4 s.

## Preparation of nanodisks

Dispersions of MLVs in solubilization buffer (Tris-HCl 50 mM, NaCl 150 mM (pH 8.0)) were mixed with SMA 10% (w/v) (SMA/lipid mass ratio ~3.0) overnight at T > $T_m$. The non-solubilized material was pelleted down by spinning at 115,000 $\times$ $g$ for 1 hr at 4°C, and the supernatant containing the solubilized lipid material was collected. Both the initial molarity and lipid composition of the dispersions of MLVs are specific for each experiment and are described as follows: nanodisk solutions measured by dynamic light scattering (DLS), and differential scanning calorimetry (DSC) analyses were obtained from initial 700 $\mu$L aliquots of 20 mM of di-14:0 PC MLVs (DLS) or di-16:0 PC MLVs (DSC). The nanodisk solutions used in rhodamine-dequenching analyses were obtained from initial 100 $\mu$L aliquots of 2 mM of di-14:0 PC/N-rhodamine di-14:0 PE (4:1 mol) MLVs.

## Differential scanning calorimetry

DSC measurements were performed using a Discovery DSC (TA Instruments, Newcastle, DE) calorimeter. 20-$\mu$L aliquots of nanodisk solutions or MLV dispersions containing ~20 mM lipids were placed in hermetic Tzero pans (TA Instruments). Heating curves were recorded in the ranges of 0–70°C at a scan rate of 5°C/min at least three times. $T_m$ values were obtained at $T_m = Cp_{max}$ using Trios software (TA Instruments). Error bars reported for $T_m$ values correspond to the average from the second and third heating cycles from two independent samples.

## Dynamic light scattering

DLS analysis was performed on the samples using a Zetasizer Nano ZS (Malvern Instruments, Worcestershire, UK). 700 $\mu$L aliquots of 20 mM of di-14:0 PC nanodisk solutions and 1 mL aliquots of SMA 1% (w/v) in buffer (Tris-HCl 50 mM, NaCl 150 mM (pH 8.0)) were measured at least 12 times, each measurement being an average of 20 subruns of 15 s. Size-intensity distributions were generated using Zetasizer software Ver. 6.20 and 7.03 and analyzed using the multiple narrow distribution. Hydrodynamic diameters were calculated from the intensity distributions with the assumption that nanodisks have a spherical shape. All samples showed a polydispersity index (PDI) < 0.3.

## Transmission electron microscopy

Size characterization of di-14:0 PC nanodisks was performed by transmission electron microscopy. Aliquots from the nanodisk solutions used for DLS analyses were diluted to a final 0.5 mM and adsorbed on carbon-coated mica following the carbon flotation technique, then stained with a staining solution containing 2% (w/v) sodium silicotungstate as detailed before (8). Images were taken under low-dose conditions at a nominal magnification of 49,000× with a T12 electron microscope (FEI, Hillsboro, OR) at an operating voltage of 120 kV using an ORIUS SC1000 camera (Gatan, Pleasanton, CA). The average size of the nanodisks was estimated from at least 10 well-defined individual particles, of which the maximal diameter was determined using Adobe Illustrator software (San Jose, CA).

## Rhodamine fluorescence dequenching

Aliquots of di-14:0 PC/N-rhodamine di-14:0 PE (4:1 mol) nanodisks were diluted to a final volume of 1 mL, yielding a final N-rhodamine di-14:0 PE concentration of 2.5 $\mu$M, and were placed in a 10-mm quartz cuvette. Next, the solutions were equilibrated for at least 2 min at 30°C by using a Peltier cuvette holder (Santa Clara, CA). Fluorescent nanodisks were excited at 560 nm and mixed with aliquots of unlabeled di-14:0 PC nanodisks. Unlabeled nanodisks were added to a final lipid molar ratio of 1:20 or 1:5 of labeled/unlabeled nanodisks. Rhodamine dequenching was monitored at 585 nm for 15 min using a Varian Cary Eclipse fluorescence spectrophotometer (Santa Clara, CA).

# RESULTS

## Commercially available SMAnh can be fractionated based on differences in solubility in hexane and acetone mixtures

SMA copolymers are obtained by hydrolysis of SMAnh copolymers, as illustrated in Fig. 1 *A*. The commercially available SMAnh copolymers are very heterogeneous and consist of a mixture of polymers with different length and composition. It can be expected that these constituents will exhibit different solubility properties in organic solvents. Although hexane and acetone are fully miscible, the polymers are soluble in acetone but insoluble in hexane. Thus, upon addition of hexane to a solution of polymer in

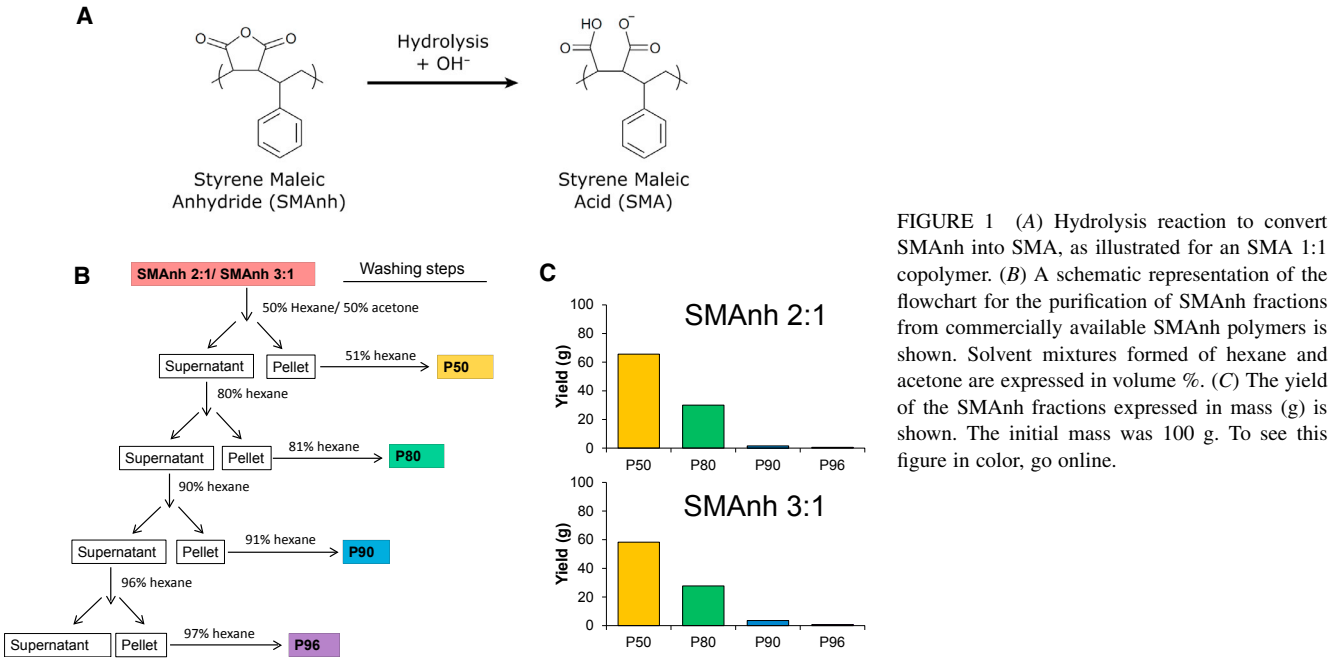


FIGURE 1 (*A*) Hydrolysis reaction to convert SMAnh into SMA, as illustrated for an SMA 1:1 copolymer. (*B*) A schematic representation of the flowchart for the purification of SMAnh fractions from commercially available SMAnh polymers is shown. Solvent mixtures formed of hexane and acetone are expressed in volume %. (*C*) The yield of the SMAnh fractions expressed in mass (g) is shown. The initial mass was 100 g. To see this figure in color, go online.

acetone, the polymers will tend to aggregate. This process may be more favorable for more hydrophilic polymers due to the decreased polarity of the medium but also for longer polymers due to entanglement of the chains. We thus set out to try and isolate subfractions of SMAnh 2:1 and SMAnh 3:1 copolymers by differential solubility in (arbitrarily chosen) mixtures of hexane and acetone. As illustrated in Fig. 1 *B*, anhydrous solutions of the polymers in acetone were initially mixed with an equal volume of hexane, yielding a two-phase system after centrifugation. The bottom phase contained a fraction of the polymer mixture, denoted the SMAnh P50 fraction, which was separated by centrifugation and washed. This procedure was repeated for a final concentration of 80% hexane, 90% hexane, and 96.5% hexane, yielding respectively the SMAnh P80, SMAnh P90, and SMAnh P96 fractions. As shown in Fig. 1 *C*, the yields for both SMAnh 2:1 and SMAnh 3:1 were highest for the SMAnh P50 and the SMAnh P80 fractions, which together contain ∼80% of the initial mass of the SMAnh.

## Separated fractions of SMAnh mixtures have different length and styrene content

The SMAnh fractions obtained were characterized by gel permeation chromatography (GPC) in organic solvent (Fig. 2, *A* and *B*), from which it was possible to determine both their $M_n$ and their PDI based on calibration with polystyrene standards (14). The $M_n$ and PDI values are displayed in Table 1. SMAnh P50 fractions were found to contain polymers with the highest $M_n$, whereas the polymers with the lowest $M_n$ were found in the SMAnh P90 fractions and in the SMAnh P96 fractions. The PDI (Table 1) was found to be smaller in the purified fractions than in the nonfractionated material, indicating a higher monodispersity.

Insight into the composition of the different SMAnh fractions was obtained by FTIR (Fig. 2, *C* and *D*). By determining the ratio between the absorbance at 680 $cm^{-1}$ ($CH_2$ = bending monosubstituted benzene) and at 1780 $cm^{-1}$ (C=O stretching, anhydride), it is possible to qualitatively compare the styrene/maleic anhydride ratios and thus to estimate the relative content of styrene present in the SMAnh fractions as compared to that in commercially available SMAnh mixtures. $A_{680\ cm-1}/A_{1780\ cm-1}$ values are displayed in Table 1.

Interestingly, $A_{680\ cm-1}/A_{1780\ cm-1}$ values obtained from SMAnh fractions indicate that the styrene content increases for those fractions that precipitated in solutions with the lowest polarity (highest hexane:acetone ratio). This was supported by ultraviolet-visible spectroscopy analysis (Fig. S2). Here it was found that SMAnh fractions consisting of polymers with the lowest $M_n$ gave the highest absorbance values in the range of 240–270 nm, typical for electronic transitions between $\pi$ and $\pi^*$ orbitals in polyene molecules. This suggests that apart from the length, polymer composition also plays a role in the solubility of the polymer. Alternatively, it is possible that the lower-$M_n$ polymer fractions contain styrene-rich contaminants or by-products that contribute to the signal.

## SMA-purified fractions yield nanodisks of approximately the same size

The samples (i.e., SMAnh) were next hydrolyzed to yield SMA. The size distributions of the SMA polymers were

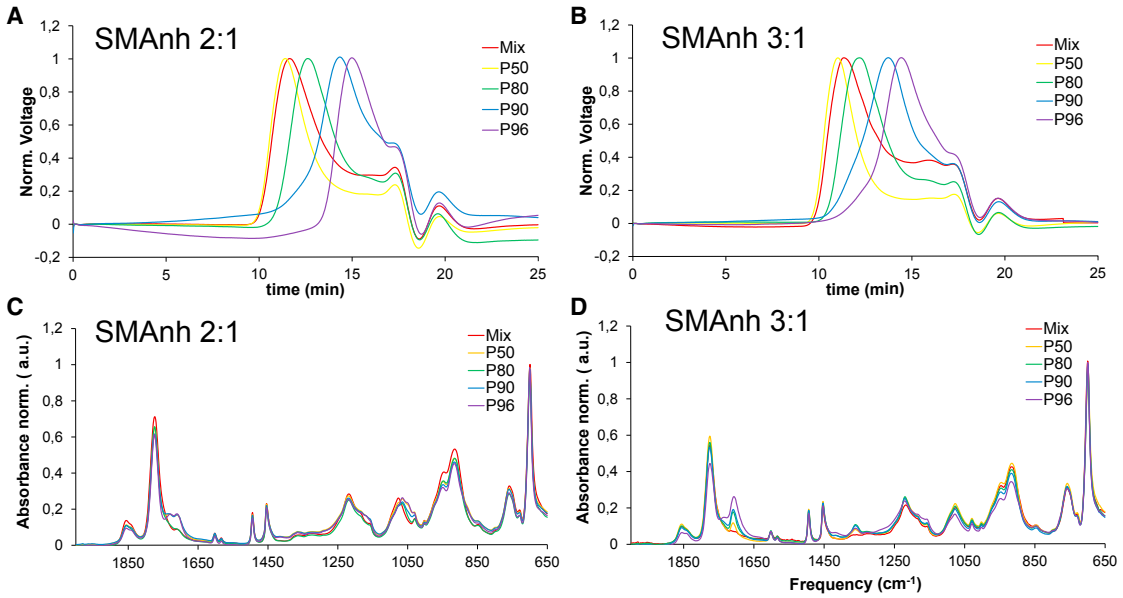


FIGURE 2 (*A*) and (*B*) GPC chromatograms of 0.2% (w/v) SMAnh 2:1 (*A*) and SMAnh 3:1 (*B*) polymers in THF. The signals at ~18–22 min of elution time are the result of changes in refractive index of the eluents due to sample injection and do not correspond to polymer fractions. (*C*) and (*D*) FTIR analyses of SMAnh 2:1 (*C*) and of SMAnh 3:1 (*D*) polymers are shown. All experiments were conducted at room temperature (~23°C). To see this figure in color, go online.

analyzed by SEC (Fig. S1) and were found to follow the same trend as those obtained by GPC (Fig. 2, *A* and *B*). Then we investigated whether all the SMA fractions are able to solubilize lipid membranes into nanodisks. Electron microscopy (EM) micrographs (Fig. 3) of solubilized lipid vesicles show that nearly all SMA fractions yield nanodisks with an average size distribution in the range of 7–10 nm. No correlation was observed between the size of the nanodisks and the $M_n$ of the polymer rim. These values are in line with the size values reported previously for similar self-assemblies (3,4,7,8). The only exception is the solubilized fraction obtained upon addition of the SMA 3:1 P96 fraction, which does not seem to contain nanodisks but micrometer-scaled particles. The nature of this self-assembly may be ascribed to the high styrene content of molecules present in the SMA 3:1 P96 fraction (Table 1), which, in conjunction with the dehydration conditions during sample preparation, leads to the formation of polymer aggregates.

**TABLE 1 Size Characterization and Composition Analysis of SMAnh Polymers**

| SMAnh 2:1 | $M_n$ (kDa) | PDI | $Abs_{680\ cm-1}/Abs_{1780\ cm-1}$ |
|---|---|---|---|
| Mix | 3.5 | 2.1 | 1.48 |
| P50 | 4.6 | 2.0 | 1.41 |
| P80 | 2.4 | 1.8 | 1.55 |
| P90 | 1.4 | 1.7 | 1.57 |
| P96 | 1.1 | 2.0 | 1.98 |
| SMAnh 3:1 | $M_n$ (kDa) | PDI | $Abs_{680\ cm-1}/Abs_{1780\ cm-1}$ |
| Mix | 4.4 | 2.1 | 1.77 |
| P50 | 6.5 | 2.0 | 1.54 |
| P80 | 3.8 | 1.6 | 1.66 |
| P90 | 1.9 | 1.7 | 1.77 |
| P96 | 1.6 | 1.6 | 2.1 |

Size characterization and composition analysis of SMAnh polymers. The $A_{680\ cm-1}/A_{1780\ cm-1}$ values are obtained from FTIR spectra represented in Fig. 1 *B*, reflecting the relative styrene-to-maleic acid ratio. The estimated error in the absorbance ratios is less than 0.04. The number-average molecular weight ($M_n$) values and polydispersity index values are obtained from the GPC spectra shown in Fig. 1 *A*. $M_n$ and PDI values are defined as $\mathbf{M_n} = \sum Ni\,Mi/\sum Ni$ and PDI= $\mathbf{M_w}/\mathbf{M_n}$, respectively, where $\mathbf{M_w} = \sum Ni\,\mathbf{Mi}^2/\sum Ni\,Mi$.

DLS measurements on nanodisks bounded by SMA 3:1-derived polymers (Fig. S3) showed similar size-distribution values as those reported by EM, in the range of 6–11 nm. For the SMA 3:1 P96 "nanodisks," an additional scattering peak was obtained at ~60 nm. This may be ascribed to the presence of insoluble membrane fragments in very low amounts, as supported by its absence in the number-intensity distribution analysis (Fig. S4). Remarkably, the nanodisks bounded by SMA 2:1-derived polymers showed a somewhat smaller average size distribution (~5–7 nm) as compared to the values obtained by EM. One should keep in mind here that the error in the DLS data reflects the position of the maximum and not the actual size distribution, which is much larger. Furthermore, as a general remark, we note that all the SMA fractions in solution (in the absence of lipids) scatter light, with an average peak maximum at ~5 nm based on number-size distribution (Fig. S5). It is thus possible that the size-distribution values are somewhat biased by the presence of free SMA.

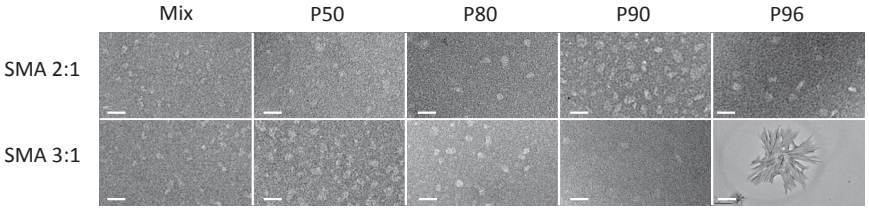


FIGURE 3 Negative-stain transmission electron micrographs of di-14:0 PC nanodisks bounded by SMA 2:1 (*top*) or SMA 3:1 (*bottom*) polymer variants. The scale bar represents 20 nm, except for the SMA 3:1 P96 micrograph, which represents 1 $\mu$m. Nanodisks were obtained at an SMA/lipid mass ratio of 3.0.

## Insertion into lipid monolayers is most efficient for SMA fractions containing shortest polymers

A crucial first step in SMA-mediated membrane solubilization is the insertion of SMA into the lipid membrane (7). The efficiency of this process was investigated for the purified SMA fractions by lipid monolayer experiments. In this case, di-18:0 PC was chosen (Fig. 4) next to conventional di-14:0 PC (Fig. S6) because it provided a more convenient window to compare differences in surface pressure increases, possibly due to its longer chains and its presence in a solid condensed phase (17). Nevertheless, similar trends were found in both lipid systems. As shown in Fig. 4, the addition of SMA fractions to the subphase of a di-18:0 monolayer leads to a fast increase in surface pressure. For both SMA 2:1 and SMA 3:1 copolymers, the surface-pressure increase is highest for the fractions containing polymers with the lowest $M_n$ values. Interestingly, a plot of the final surface-pressure values as function of the $M_n$ of the SMA polymers suggests a linear relationship (Fig. 4 *C*). Here, the styrene content does not seem to play a role, as very similar values are found for SMA 2:1 and SMA 3:1 fractions.

## Solubilization of lipid bilayers is most efficient for SMA fractions containing the shortest polymers

Next, the kinetics and efficiency of membrane solubilization by the SMA fractions were investigated using di-14:0 PC vesicles at a temperature below the $T_m$, as described previously (7,11). As shown in Fig. 5, *A* and *B*, the solubilization rates appear to follow the same trend as observed for the insertion of the SMA fractions into lipid monolayers, with low-$M_n$ SMA polymers solubilizing vesicles more efficiently than high-$M_n$ SMA polymers. As with the surface pressure isotherms, the final turbidimetry values also appear to hold a linear relation with the $M_n$ values of the SMA fractions regardless of the monomer composition of the polymer (Fig. 5 *C*). These findings suggest that the length of SMA plays the most important role in both the insertion of SMA into a lipid surface and in the subsequent solubilization of the membrane, regardless of the overall styrene/maleic acid ratio.

## Nanodisks bounded by long SMA molecules exhibit slower lipid exchange rates than those bounded by short SMA molecules

Next, the importance of SMA polymer length for the stability of the nanodisks was investigated by monitoring the lipid exchange rates. These were studied by making use of the concentration-dependent fluorescence properties of rhodamine. The dye was incorporated at self-quenching concentrations in lipid nanodisks bounded by different SMA 2:1 and SMA 3:1 fragments, and the increase in fluorescence was monitored upon addition of rhodamine-free nanodisks. A possibly complicating factor here is that the initial rhodamine fluorescence in nanodisks at $t = 0$ s seemed to be affected by the length of the SMA belt (Fig. S7), being lower for those bounded by low-$M_n$ SMA polymers. By contrast, the final fluorescence values appeared to be independent of the polymer length. The reason for these differences is not clear, but it may be related to the high extent of membrane insertion of low-$M_n$ polymers, as will be discussed later.

As shown in Fig. 6 *A*, nanodisks bounded by SMA 2:1 fractions containing the longest polymers (SMA 2:1 P50) exhibit the slowest dequenching rates upon the addition of empty nanodisks, thus indicating the slowest lipid exchange rates between nanodisks. Dequenching occurs faster when the length of the polymer becomes smaller, as illustrated in Fig. 6 *C*, in which the time required to achieve 50% of total dequenching ($t_{0.5}$) is plotted against the $M_n$ value of the polymer belts. Remarkably, very fast dequenching rates were observed for nanodisks bounded by SMA 3:1-derived polymers (Fig. 6 *B*), in line with previous reports (18). Despite the fast lipid exchange rates observed between SMA 3:1-nanodisks, it was possible to detect slower dequenching rates for nanodisks bounded by high-$M_n$ polymers than for those bounded by low-$M_n$ polymers. The clear differences in lipid exchange rates between nanodisks bounded by polymers derived from SMA 2:1 and from SMA 3:1 commercial blends are in line with results from a recent report (19) and may be ascribed to the lower thermodynamic stability of SMA 3:1-nanodisks (9), making them more susceptible to undergoing the dynamic changes required for lipid exchange.

As a final remark, notably slower lipid exchange rates were obtained when the total excess of empty nanodisks in solution was lowered by a factor of four (Fig. S8). This finding may serve to support the theory that lipid

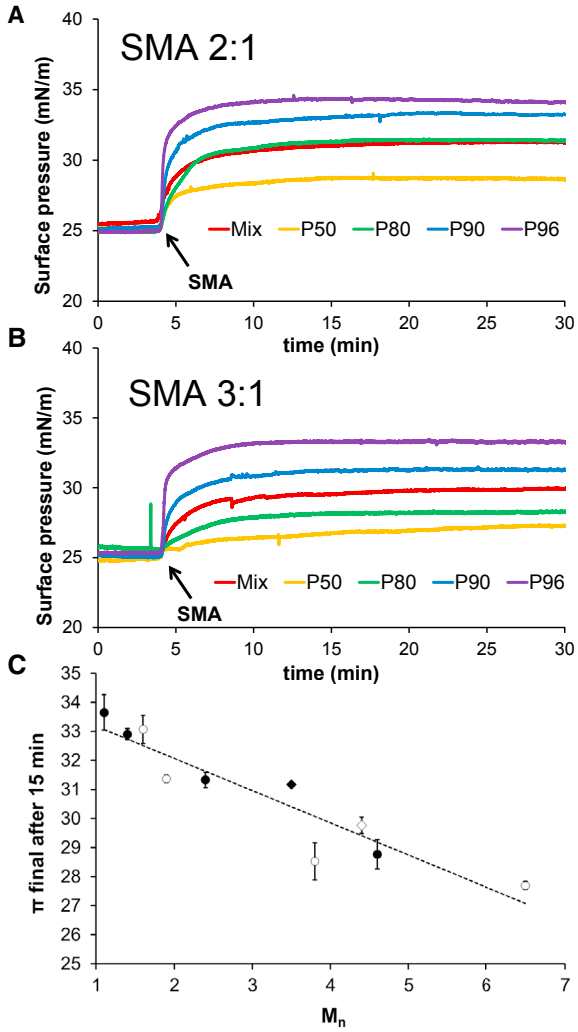


FIGURE 4 Surface-pressure increase in monolayers composed of di-18:0 PC induced by the insertion of SMA copolymer fractions obtained from commercial mixtures consisting of SMA 2:1 (*A*) or SMA 3:1 (*B*). All surface pressure isotherms were recorded for at least 30 min at room temperature (~23°C). (*C*) The final surface-pressure values ($t$ = 30 min) are plotted against the $M_n$ of the SMA fractions. Full circles correspond to SMA fractions purified from commercial SMA 2:1 mixtures, and empty circles to those purified from commercial SMA 3:1 mixtures. SMA mixtures are indicated by diamonds. Error bars represent the range in at least two independent experiments. To see this figure in color, go online.

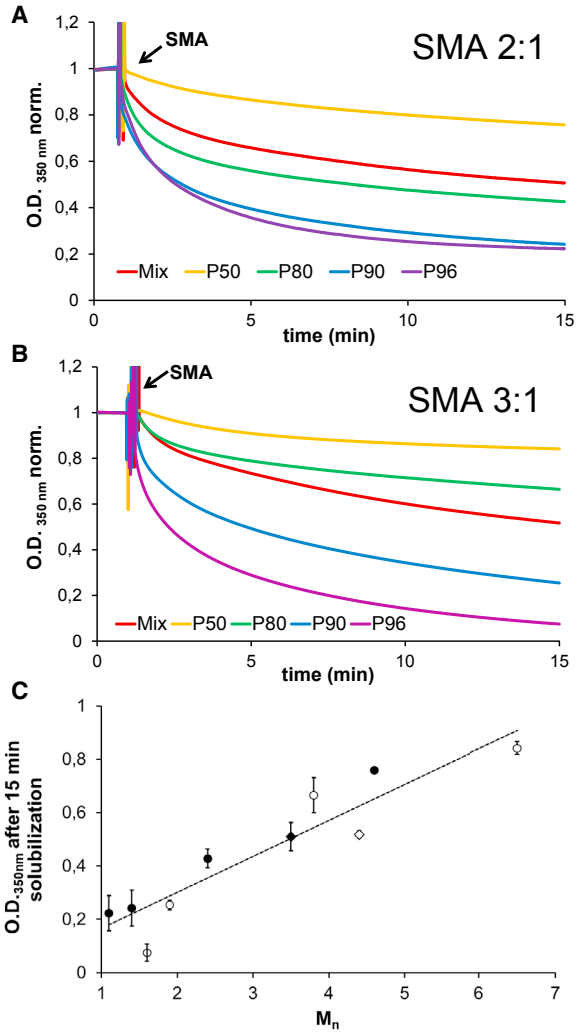


FIGURE 5 Solubilization kinetics of 0.5 mM di-14:0 PC MLVs induced by SMA copolymer fractions obtained from commercial mixtures consisting of SMA 2:1 (*A*) or SMA 3:1 (*B*). Solubilization was conducted at 15°C at an SMA/lipid mass ratio of ~3. Data are shown as normalized optical density at 350 nm. (*C*) Final $OD_{350\ nm}$ values ($t$ = 30 min) are plotted against the $M_n$ of the SMA fractions. Full circles correspond to SMA fractions purified from commercial SMA 2:1 mixtures, and empty circles to those purified from commercial SMA 3:1 mixtures. SMA mixtures are indicated by diamonds. Error bars represent the range in at least two independent experiments. To see this figure in color, go online.

exchange between nanodisks shows a high Brownian dependence, thus being affected by the number of particles in solution (18).

## Lipids in nanodisks encircled by long SMA 2:1 molecules retain to a higher extent their native thermotropic properties than those encircled by small SMA molecules

The thermodynamic stability of nanodisks was further investigated by analyzing the thermotropic properties of the lipids embedded in them. Fig. 7 *A* shows that the $T_m$ of di-16:0 PC lipids in nanodisks bounded by SMA 2:1 mixture is downshifted ~7°C as compared to that in MLVs ($T_m$ values are displayed in Table S1). Furthermore, a decrease in both the cooperativity and in the calorimetric enthalpy of the gel-to-fluid phase transition in SMA 2:1 nanodisks can be observed as compared to that in vesicular self-assemblies, in line with results from previous studies (9,10). Nanodisks bounded by SMA 2:1 fractions containing high-$M_n$ polymers exhibit similar downshifts in $T_m$ as those bounded by the commercial SMA 2:1 mixture and thus perturb the thermodynamic equilibrium of the membrane the least. By contrast, lipids encircled by SMA 2:1

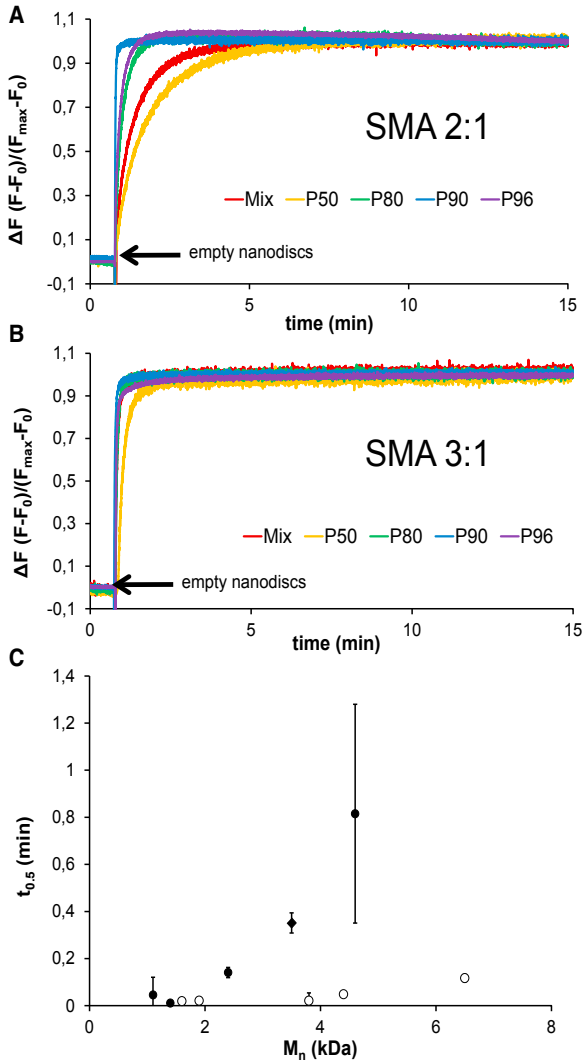


FIGURE 6 Dequenching of rhodamine-PE in d-14:0 PC nanodisks (20% mol rhodamine) with time upon addition of unlabeled nanodisks. Nanodisks are bounded by SMA polymers obtained from commercial SMA 2:1 mixtures (*A*) or from SMA 3:1 mixtures (*B*). The figure includes a plot of the time required to achieve 50% of total lipid exchange ($t_{0.5}$) as a function of the number-average molecular weight of the polymer (*C*). Full circles correspond to SMA fractions purified from commercial SMA 2:1 mixtures, and empty circles to those purified from commercial SMA 3:1 mixtures. SMA mixtures are indicated by diamonds. Nanodisks were obtained at an SMA/lipid mass ratio of ~3 and mixed in a ratio (mol) of 20:1 empty nanodisks/fluorophore-loaded. Fluorescence dequenching was recorded for 15 min at $\lambda_{em} = 585$ nm at 30°C. Error bars represent the range in at least two independent experiments. To see this figure in color, go online.

fractions containing low-$M_n$ polymers showed a poor retention of the native thermotropic properties by the lipids. For example, the $T_m$ value of di-16:0 PC lipids in nanodisks bounded by polymers from the SMA 2:1 P90 fraction is downshifted ~22°C as compared to that in MLVs. Furthermore, the thermogram corresponding to di-16:0 PC encircled in nanodisks bounded by SMA 2:1 P96 shows a transition that is extensively broadened

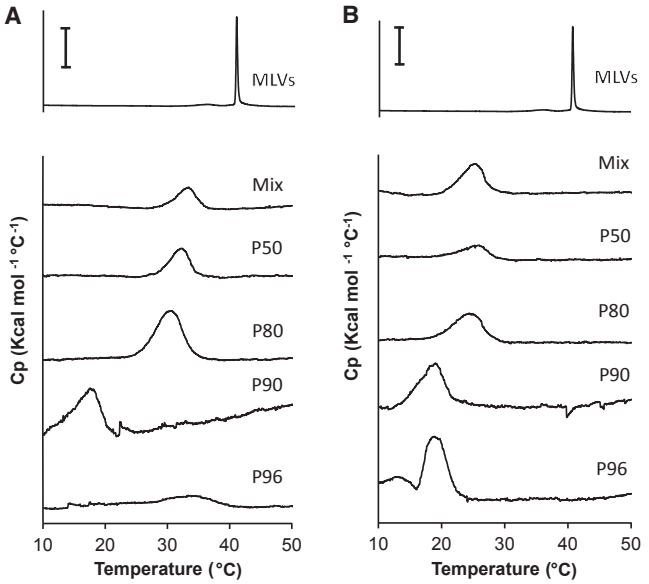


FIGURE 7 Representative DSC thermograms of di-16:0 PC lipids self-assembled in either MLVs (*top*) or in nanodisks bounded by SMA 2:1-derived polymers (*A*) or by SMA 3:1-derived polymers (*B*). Nanodisks were obtained at an SMA/lipid mass ratio of ~3.0. The inserted scale bars at the top represent 5 kcal/mol °C for the thermograms consisting of MLVs and to 0.5 kcal/mol °C for the thermograms consisting of nanodisks.

and hardly detectable, suggesting that lipids are largely removed from the phase transition.

As shown in Fig. 7 *B*, the native thermotropic properties of the enclosed lipids are overall less well retained in nanodisks bounded by SMA 3:1-derived polymers. This is indicated by more pronounced downshifts in $T_m$, in line with recent findings (9). A similar trend is observed for the thermograms corresponding to nanodisks bounded by SMA 3:1-derived fragments as found for SMA 2:1-derived fragments. Overall, lipids encircled by nanodisks bound by low-$M_n$ SMA retain the native thermotropic properties the least. Nanodisks bounded by SMA 3:1 P96 polymers seem to undergo an additional transition, which has recently been ascribed to an energetic contribution of the SMA polymer during the melting transition of the lipids, possibly related to the poor thermodynamic stability of the nanodisk particles (9). Overall, these results suggest that nanodisks are more stable when bounded by long SMA polymers.

## DISCUSSION

In recent years, the solubilization of lipid membranes by SMA copolymers has been studied extensively using model membrane systems. These studies were assessed with commercial SMA mixtures that are highly heterogeneous, thus hampering our molecular understanding of SMA-lipid interactions. Several studies suggested that polymer size is important for solubilization and properties of the nanodisks (11–13). Here, we present a simple method to separate

high-$M_n$ and low-$M_n$ SMA copolymers from commercial SMAnh blends. It was found by EM analysis that all the SMA fractions except SMA 3:1 P96 were able to yield circular nanodisks with a size of ~7–10 nm. Neither EM nor DLS measurements showed a correlation between the size of the nanodisks and the $M_n$ of the polymer rim.

By investigating the interaction of SMA fractions with phosphatidylcholine self-assemblies, it was found that low-$M_n$ polymers are most efficient in membrane insertion and membrane solubilization. The most straightforward explanation for this behavior is that for long polymers, it is sterically more difficult to cover a large membrane area while at the same time achieving insertion of all hydrophobic phenyl groups. The fast solubilization by low-$M_n$ copolymers could be an important advantage when using SMA for isolation and purification of membrane proteins from biological membranes. For example, the potentially increased efficiency may result in an increase in yield, or it may reduce the exposure time of the protein to potentially harsh conditions. In addition, the use of low-$M_n$ copolymers may make it easier to separate excess polymers from nanodisk preparations, e.g., by filtration or SEC.

Our results furthermore show that the use of low-$M_n$ polymers also has a potential disadvantage. Lipids in nanodisks bounded by low-$M_n$ polymers were found to exhibit faster exchange rates between lipids in neighboring nanodisks, as concluded from fluorescence dequenching of rhodamine-labeled lipids in nanodisks upon addition of nanodisks with unlabeled lipids. Furthermore, lipids enclosed by low-$M_n$ polymers showed less retention of the native thermotropic properties than those enclosed by high-$M_n$ polymers based on DSC measurements. Because low-$M_n$ polymers insert more efficiently into lipid monolayers, it is possible that in the nanodisks they not only shield the hydrophobic lipid acyl chains from the aqueous environment but also insert between the lipid headgroups on both surfaces of the nanodisks. Thereby they will cause more disruption of native lipid-lipid interactions, thus decreasing thermodynamic stability.

We also compared the behavior of SMA 3:1 fractions with that of SMA 2:1 fractions. Both polymer fractions showed rather similar behavior in terms of insertion and solubilization. However, SMA 3:1 fractions yielded overall less stable nanodisks than SMA 2:1 fractions, in agreement with results from previous studies on SMA mixtures (9–11) This behavior has been ascribed to the higher styrene content and/or to the higher chance of obtaining consecutive styrene monomer sequences in the polymer-growing chain for SMA 3:1 (9,11), which could result in a less homogeneous packing of the polymers around the rims of the nanodisks.

In conclusion, we have shown that the length of SMA copolymers is a key parameter in membrane solubilization and in determining properties of the resulting nanodisks. This knowledge may help in optimizing conditions for isolation and characterization of membrane proteins from native membranes, depending on which properties are considered most relevant for a particular purpose, e.g., solubilization yield or stability of the nanodisks. However, we wish to emphasize that the polymer-length-dependent effects observed in this study may not necessarily be the same in biological membranes, in which the heterogeneous composition of proteins and lipids may further affect both solubilization efficiency and stability.

## SUPPORTING MATERIAL

Eight figures and one table are available at http://www.biophysj.org/biophysj/supplemental/S0006-3495(18)30671-4.

## AUTHOR CONTRIBUTIONS

J.J.D.P., M.C.K., and J.A.K. designed the project. M.C.K. prepared polymer fragments. J.J.D.P., N.U., and J.W. conducted experiments consisting of SEC, monolayer insertion, membrane solubilization, FTIR, and DLS. J.J.D.P. and A.H.K. conducted calorimetric analyses and lipid-exchange experiments. M.J.v.S. conducted GPC measurements. J.J.D.P., C.A.v.W., and H.J. analyzed the data. J.J.D.P. and J.A.K. wrote the article with input from all other coauthors.

## ACKNOWLEDGMENTS

We thank Jonas M. Dörr and Stefan Scheidelaar (both from University of Utrecht, The Netherlands) and Bert Klumperman (Stellenbosch University, South Africa) for helpful discussions. We are very grateful to Christine Moriscot, Guy Schoehn, and Daphna Fenel, all from the EM platform of the Integrated Structural Biology of Grenoble (UMI3265) for performing the transmission electron microscopy imaging.

This work was supported financially by NWO Chemical Sciences, ECHO grants No. 711-013-005 (J.J.D.P) and No. 711-017-006 (A.H.K). This work used the platforms of the Grenoble Instruct Centre (UMS 3518 CNRS-CEA-UJF-EMBL) with support from French Infrastructure for Integrated Structural Biology (ANR-10-INSB-05-02) and Grenoble Alliance for Integrated Biology (ANR-10-LABX-49-01) within the Grenoble Partnership for Structural Biology.

## REFERENCES

1. Dörr, J. M., S. Scheidelaar, …, J. A. Killian. 2016. The styrene-maleic acid copolymer: a versatile tool in membrane research. *Eur. Biophys. J.* 45:3–21.
2. Esmaili, M., and M. Overduin. 2018. Membrane biology visualized in nanometer-sized discs formed by styrene maleic acid polymers. *Biochim. Biophys. Acta.* 1860:257–263.
3. Orwick, M. C., P. J. Judge, …, A. Watts. 2012. Detergent-free formation and physicochemical characterization of nanosized lipid-polymer complexes: Lipodisq. *Angew. Chem. Int.Engl.* 51:4653–4657.
4. Jamshad, M., V. Grimard, …, T. R. Dafforn. 2015. Structural analysis of a nanoparticle containing a lipid bilayer used for detergent-free extraction of membrane proteins. *Nano Res.* 8:774–789.
5. Ravula, T., S. K. Ramadugu, …, A. Ramamoorthy. 2017. Bioinspired, size-tunable self-assembly of polymer-lipid bilayer nanodiscs. *Angew. Chem. Int.Engl.* 56:11466–11470.

6. Vargas, C., R. C. Arenas, …, S. Keller. 2015. Nanoparticle self-assembly in mixtures of phospholipids with styrene/maleic acid copolymers or fluorinated surfactants. *Nanoscale.* 7:20685–20696.
7. Scheidelaar, S., M. C. Koorengevel, …, J. A. Killian. 2015. Molecular model for the solubilization of membranes into nanodisks by styrene maleic Acid copolymers. *Biophys. J.* 108:279–290.
8. Dominguez Pardo, J. J., J. M. Dörr, …, J. A. Killian. 2017. Solubilization of lipids and lipid phases by the styrene-maleic acid copolymer. *Eur. Biophys. J.* 46:91–101.
9. Dominguez Pardo, J. J., J. M. Dörr, …, J. A. Killian. 2017. Thermotropic properties of phosphatidylcholine nanodiscs bounded by styrene-maleic acid copolymers. *Chem. Phys. Lipids.* 208:58–64.
10. Grethen, A., A. O. Oluwole, …, S. Keller. 2017. Thermodynamics of nanodisc formation mediated by styrene/maleic acid (2:1) copolymer. *Sci. Rep.* 7:11517.
11. Scheidelaar, S., M. C. Koorengevel, …, J. A. Killian. 2016. Effect of polymer composition and pH on membrane solubilization by styrene-maleic acid copolymers. *Biophys. J.* 111:1974–1986.
12. Swainsbury, D. J. K., S. Scheidelaar, …, M. R. Jones. 2017. The effectiveness of styrene-maleic acid (SMA) copolymers for solubilisation of integral membrane proteins from SMA-accessible and SMA-resistant membranes. *Biochim. Biophys. Acta.* 1859:2133–2143.
13. Morrison, K. A., A. Akram, …, A. J. Rothnie. 2016. Membrane protein extraction and purification using styrene-maleic acid (SMA) copolymer: effect of variations in polymer structure. *Biochem. J.* 473:4349–4360.
14. Saldívar-Guerra, E., and E. Vivaldo-Lima. 2013. Handbook of Polymer Synthesis, Characterization, and Processing. John Wiley & Sons, Inc, Hoboken, NJ.
15. Rouser, G., S. Fkeischer, and A. Yamamoto. 1970. Two dimensional then layer chromatographic separation of polar lipids and determination of phospholipids by phosphorus analysis of spots. *Lipids.* 5:494–496.
16. Lewis, R. N., N. Mak, and R. N. McElhaney. 1987. A differential scanning calorimetric study of the thermotropic phase behavior of model membranes composed of phosphatidylcholines containing linear saturated fatty acyl chains. *Biochemistry.* 26:6118–6126.
17. Boisselier, É., P. Calvez, …, C. Salesse. 2012. Influence of the physical state of phospholipid monolayers on protein binding. *Langmuir.* 28:9680–9688.
18. Cuevas Arenas, R., B. Danielczak, …, S. Keller. 2017. Fast collisional lipid transfer among polymer-bounded nanodiscs. *Sci. Rep.* 7:45875.
19. Grethen, A., D. Glueck, and S. Keller. 2018. Role of Coulombic repulsion in collisional lipid transfer among SMA(2:1)-bounded nanodiscs. *J. Membr. Biol* https://doi.org/10.1007/s00232-018-0024-0.